In Vivo Entombment of Bacteria and Fungi during Calcium Oxalate, Brushite and Struvite Urolithiasis

Saw JJ[1,2,3†], Sivaguru M[1†], Wilson EM[1,4], Dong Y[1], Sanford RA[1,5], Fields CJ[6], Cregger MA[1,7], Merkel AC[1,4], Bruce WJ[1,4], Weber JR[1,4], Lieske JC[8,9], Krambeck AE[10,11], Rivera ME[11], Large T[11], Lange D[12], Bhattacharjee, AS[1], Romero MF[13,14], Chia N[9,10], and Fouke BW[1,4,5,6*]

[1]Carl R. Woese Institute for Genomic Biology, University of Illinois at Urbana-Champaign, Urbana, Illinois, USA.
[2]Department of Molecular and Integrative Physiology, University of Illinois at Urbana-Champaign, Urbana, Illinois, USA.
[3]Mayo Clinic Alix School of Medicine, Mayo Clinic, Rochester, Minnesota, USA.
[4]School of Molecular and Cellular Biology, University of Illinois at Urbana-Champaign, Urbana, Illinois, USA.
[5]Department of Geology, University of Illinois at Urbana-Champaign, Urbana, Illinois, USA.
[6]Roy J. Carver Biotechnology Center, University of Illinois at Urbana-Champaign, Urbana, Illinois, USA.
[7]Biosciences Division, Oak Ridge National Laboratory, Oak Ridge, Tennessee, USA.
[8]Department of Nephrology and Hypertension, Mayo Clinic, Rochester, Minnesota, USA
[9]Department of Laboratory Medicine and Pathology, Mayo Clinic, Rochester, Minnesota, USA
[10]Department of Urology, Mayo Clinic, Rochester, Minnesota, USA
[11]Department of Urology, Indiana University School of Medicine, Indianapolis, Indiana, USA.
[12]The Stone Centre at Vancouver General Hospital, Department of Urologic Sciences, University of British Columbia, Jack Bell Research Centre, Vancouver, British Columbia, Canada.
[13]Department of Individualized Medicine, Mayo Clinic, Rochester, Minnesota, USA.
[14]Department of Physiology & Biomedical Engineering, Mayo Clinic, Rochester, MN, USA.

[†]*Joint First Authors:* Jessica J. Saw and Mayandi Sivaguru
**Corresponding Author:* Bruce W. Fouke; fouke@illinois.edu

Supplementary Materials

I. Supplementary Methods

Kidney Stone Collection. All patients received antibiotics for a minimum of 7 days before surgery. Stones were removed during surgery per normal PCNL protocol by A. Krambeck at the Mayo Clinic and divided into four subsets for: (1) standard clinical anaerobic culturing, (2) infrared spectrum analysis for bulk mineralogical analysis (Table S3), (3) petrographic thin sectioning and imaging analysis, and (4) 16S rRNA gene sequence and ITS sequencing analysis. Stone sample subsets for imaging and sequencing analyses were snap frozen immediately after surgical removal, placed in sterile conical centrifuge tubes, and kept in a Taylor-Wharton CX Series dry shipper dewar (Borehamwood, UK). Frozen samples were shipped in dry ice overnight to the Fouke Lab at the University of Illinois Urbana Champaign and kept frozen at -80°C. Kidney stones were then thawed and homogenized with a sterile mortar and pestle under sterile laminar flow hood conditions genomic DNA extraction

Patient Metadata. This basic medical research study was reviewed and approved by the Institutional Review Board (IRB 09-002083) at the Mayo Clinic. Written informed consent was obtained from all participants. Approximately six weeks after stone removal, patients completed a metabolic evaluation for stone disease, which included 24-hour urine collection for supersaturation profile (EQUIL2). Medical history, standard serum labs, medication intake (e.g. citrate, thiazides, allopurinol), and comorbid conditions (e.g. diabetes mellitus, obesity, gout, hypertension, distal rental tubular acidosis, malabsorption-related conditions and diseases) were assessed from the medical record (Table S1). A 24-hour supersaturation profile was obtained from all patients after surgery (EQUIL2).

IR Spectroscopy. All stones were analyzed for bulk mineralogical composition in the Mayo Clinic Metals Laboratory (Table S3). IR spectroscopy was performed on all stones as described previously(1). While it is understood that most kidney stones are composed of multiple types of minerals(2), Fourier transform infrared (FTIR) spectroscopy determined that this cohort of 20 patients included 18 calcium oxalate (CaOx) stone formers, one brushite stone former and one struvite stone former. These classifications were based off of standardized clinical methodology(2) where stones comprised of more than 80% of either CaOx, brushite or struvite were named "CaOx," "struvite" and "brushite" stones, respectively. This 90% CaOx, 10% brushite and 10% struvite apportionment of kidney stone mineralogies in the present study closely reflects the overall distribution of human kidney stone mineralogies observed worldwide(3).

16S rRNA Gene Sequence and ITS Amplification and Sequencing. Genomic DNA was extracted using the PowerSoil DNA Isolation Kit (*MoBio Laboratories, Inc., CA*). DNA of each sample was dissolved in 30-50 µL elution buffer and quantified using an ND 1000 NanoDrop (*Thermo Scientific, Wilmington, DE*). Amplification of the targeted genes was conducted by PCR using Kapa HiFi PCR kits (KAPABiosystems, Wilmington, MA). The DNA Engine Thermal Cycler (BioRad Life Science, Hercules, CA) was programmed for 45s at 98°C, followed by 25 cycles of 15s at 98°C, 30s at 65°C, and 30s at 72°C, followed by 2 minutes at 72°C. PCR products were purified using the QIAquick PCR Purification Kit (Qiagen Inc., Valencia CA). Purified products were quantified using a Qubit 2.0 Fluorometer (Life Technologies, Grand Island, NY) and pooled at equal concentrations. Samples were run on a 1.5% agarose gel and gel extracted using a

QIAquick Gel Extraction Kit (Qiagen Inc., Valencia CA) and then sequenced using the Illumina MiSeq platform.

Microbial communities were identified using the F28/R519 and F357/R926 primers that targeted the V1-V3 and V3-V5 hypervariable regions of the 16S rRNA gene sequences for bacteria, ITS1/ITS4 and ITS3/ITS4 primers that targeted the ITS1 and ITS2 regions of the eukaryotic DNA for fungi, and Arch349F/806R primers to target archaea. Sequences were denoised, analyzed and correlated to patient metadata using DADA2, phyloseq v1.22.3 and R software. Reads from the Arch349F/806R primers were below detection limits.

Fluidigm sequences were denoised and analyzed with the software package DADA2 version 1.8(4). Samples with a sharp drop in quality within the first 100 cycles were removed from analysis. After primer trimming, forward and reverse reads were truncated so that final read length was 223 and 132 basepairs, respectively. Reads with any ambiguous bases and expected errors greater than two were removed. If the DADA2 algorithm detected a nucleotide with expected error of two or less, the remaining portion of the read was truncated. Finally, reads that matched against the phiX genome were removed. The remaining samples were dereplicated then run through the core DADA2 error correction algorithm. The resulting sequences are PCR error-corrected amplicon sequence variants (ASVs), which are analogous to operational taxonomic units (OTUs). Since combined forward and reverse read length was shorter than the expected length of the total target amplicon sequence, forward and reverse reads were concatenated, with a 10N spacer inserted between each forward and reverse read. Forward only reads were analyzed and compared against the concatenated reads and results were similar. In the final step of preprocessing, all chimeras were removed.

Bacterial and archaeal ASVs were aligned against the SILVA 16S database v132(5). Fungal ASVs were aligned against the UNITE ITS database(6). All alignments were completed to the species level if possible. All reads classified as Eucarya at the domain level were intentionally kept for analysis to determine the composition of all genetic material embedded in the stone. Eucarya reads were aligned to the BLAST nucleotide database. If there was no match, eukaryotic reads were referenced against human chromosome Human Genome, GRCh38.p12 reference, Annotation Release 109 and classified as host non-ribosomal DNA. Reads aligning to host non-ribosomal DNA were retained for analyses. Reads aligning to Cyanobacteria/chloroplast were filtered.

Community diversity and patient metadata analyses utilizing the V3-V5 16S rRNA gene sequence hypervariable and ITS2 region gene libraries are presented in the results. These libraries exhibited higher read quality and counts than V1-V3 and ITS1 amplicon libraries (Table S3, Figures S2-3). A set of 11 empty control samples containing only the DNA extraction and sequencing reagents were run through the DNA extraction and sequencing pipeline as described above. All ASVs present in the control samples were identified as contaminants. Contaminant ASVs identified in a kidney stone sample were removed not included in any results reported. Diversity analysis and all subsequent statistical analysis was completed using phyloseq package v1.22.3(7) and R statistical package(8). Statistical correlations in microbial community presence and patient metadata was assessed using Wilcoxon signed-rank and Fisher's exact test. P-values < 0.05 were considered statistically significant.

Preparation of Petrographic Thin Sections. Using a Zeiss Axiozoom. V16 Microscope (Carl Zeiss, Oberkochen, Germany), a line of section for thin section preparation was chosen along an orientation that would allow for visualization of all stages of stone growth within the complete thin section. Whole stone photographs and descriptions were sent with each stone to Wagner Petrographic Ltd. in Linden, Utah. Wagner prepared standard size (24 mm x 46 mm), uncovered (no cover slip), doubly polished thin sections. After vacuum impregnation, slides were mounted on borate silicate glass slides using clear low-viscosity cathodoluminescence-resistant epoxy impregnation, which completed preparation of the double-sided polished, 25 µm-thick petrographic thin sections.

Thin section microscopy (BF, TPMT, SRAF and Raman Spectroscopy). Sections were imaged using several optical modalities. Brightfield images of the kidney whole stones and their corresponding thin sections were taken on a Zeiss Axio Zoom.V16 microscope with a 1.0x Plan Apochromat NA 0.25 objective. The samples were illuminated with a DL 450 LED light source base and imaged with a pair of circular polarizers (CPOL) to image the crystal birefringence using a Zeiss Axiocam 512 color camera (Carl Zeiss, Oberkochen, Germany). In addition, a Zeiss Axio Observer Widefield System was used with a 63X Plan-Apochromat (1.4 NA) objective to image high-resolution BF and POL (crossed pols) from thin sections using the same Zeiss Axiocam 512 color camera (Carl Zeiss, Oberkochen, Germany). Super-resolution (~140nm) images of autofluorescence were collected using a Zeiss LSM 880 Laser Scanning Microscope with an Airyscan Super-Resolution system(1, 9, 10) using 405 (emission collected between 410-460 nm; pseudo-colored blue), 488 (emission collected between 500-550; pseudo-colored green) and 561 (emission collected between 570-615 nm; pseudo-colored red) nm excitation wavelengths. The images presented are these three RGB channels merged to form super resolution autofluorescence (SRAF) images. In addition, transmitted light photomultiplier (TPMT) images (black and white) were also taken at the same locations to show the crystalline architecture. The images of both SRAF and TPMT are overlaid with changes in opacity to show the locations of autofluorescence, especially from entombed bacteria in the context of crystalline architecture. In addition, a WITec Alpha 300RA AFM-Raman-SNOM system has been used to collect detailed Raman maps. An UHTS 600 VIS spectrometer (600 mm focal length) was used for enhanced sensitivity and better peak separation. Using a large area as well as image scan options, an area more than the field of view was tiled and stitched using a 100x Plan Neofluar (0.95 NA) objective at 150 points per line and 0.1s integration time. The Raman maps and spectra were background subtracted using the Project 5 WITec software and components were extracted automatically. The color-coded mineral components were correlatively overlaid on high resolution brightfield images acquired in a widefield microscope system. This yielded a high resolution Raman overlay producing a correlative microscopy and spectroscopy of the same location from two different systems (Fig. 7). The acquired Raman peaks were confirmed with the published Raman spectroscopy for struvite, hydroxyapatite and lipids(11, 12).

All images were processed using the Zeiss Zen Blue and/or Black software to display either maximum or minimum best-fit properties unless noted. Additionally, red-green-blue (RGB) curves were adjusted manually and individually to highlight crystal intensity within individual frames of the whole section. When necessary, a non-linear gamma correction of 1.45, 0.45 of 0.70 was applied where appropriate to further enhance difficult to visualize AF crystals using the same Zen program within the spline display mode property. All other corrections are presented within

corresponding figure legends following the protocols described in Cromey et al.(13). Final images were cropped, overlaid, resized and assembled using Adobe Photoshop (Adobe Systems Inc., San Jose, CA) to fit the required format.

II. Supplementary Figures

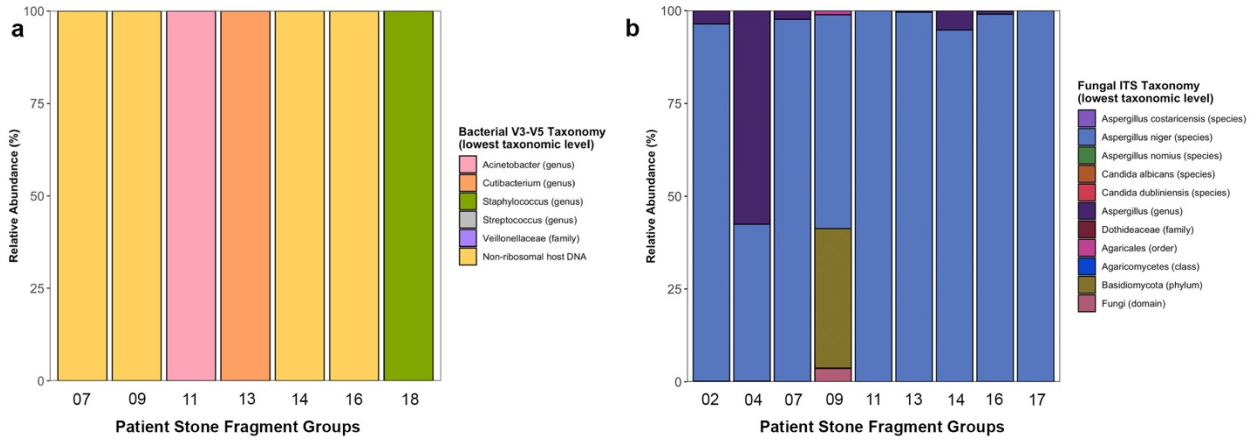

Figure S1. Relative Abundance for Individual CaOx Stones. (**a**) Bacterial V3-V5 amplicon sequencing community composition for each CaOx patient stone fragment group (n = 7 patients). (**b**) Fungal ITS2 amplicon sequencing community composition for each CaOx patient stone fragment group (n = 9 patients).

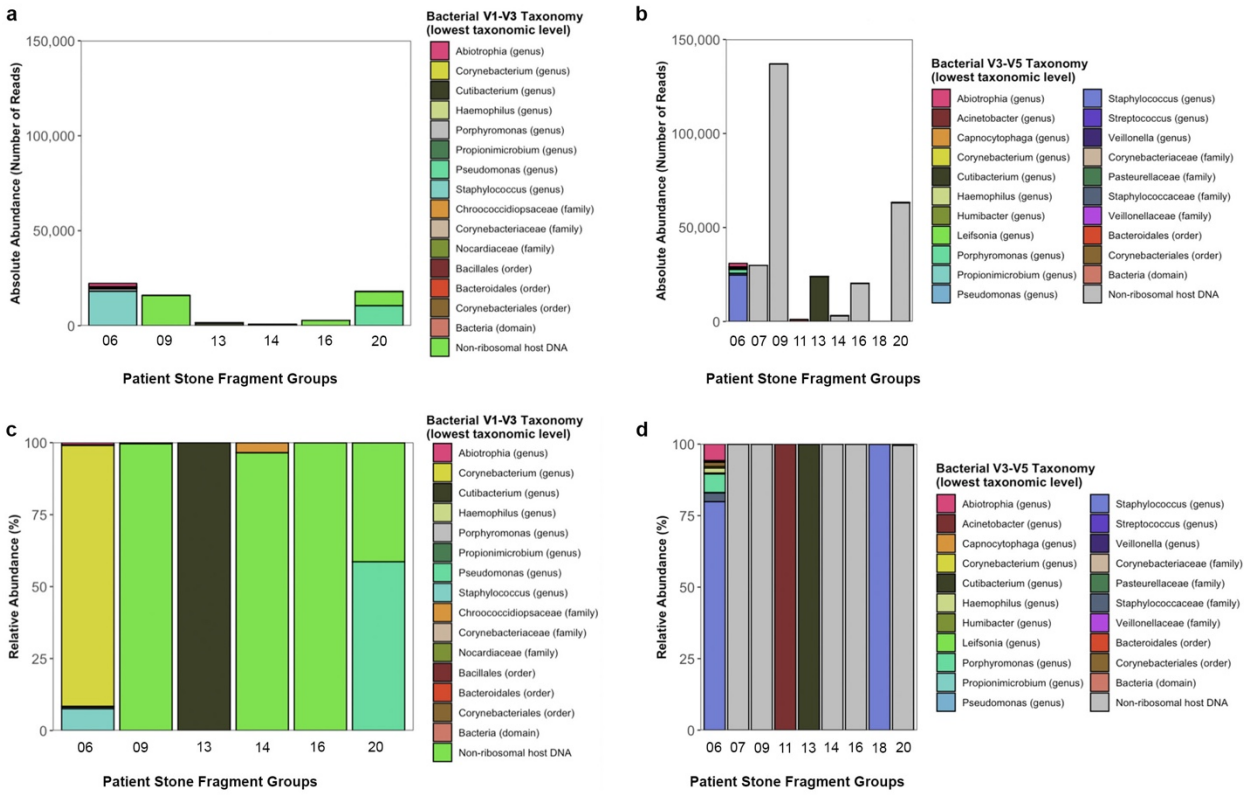

Figure S2. Comparison of 16S rRNA bacterial amplicon gene sequencing (V1-V3 versus V3-V5 hypervariable region). Reads were identified in 6 stone fragment groups in the V1-V3 amplicon sequencing versus 9 stone fragment groups in the V3-V5 amplicon sequencing. Each individual stone fragment group is represented by an identification number (x-axis). (**a**, **b**) Absolute abundance of reads for each individual stone fragment group utilizing the V1-V3 (**a**) and V3-V5 (**b**) hypervariable regions. (**c**, **d**) Relative abundance of reads for each individual patient utilizing the V1-V3 (**c**) and V3-V5 (**d**) hypervariable regions.

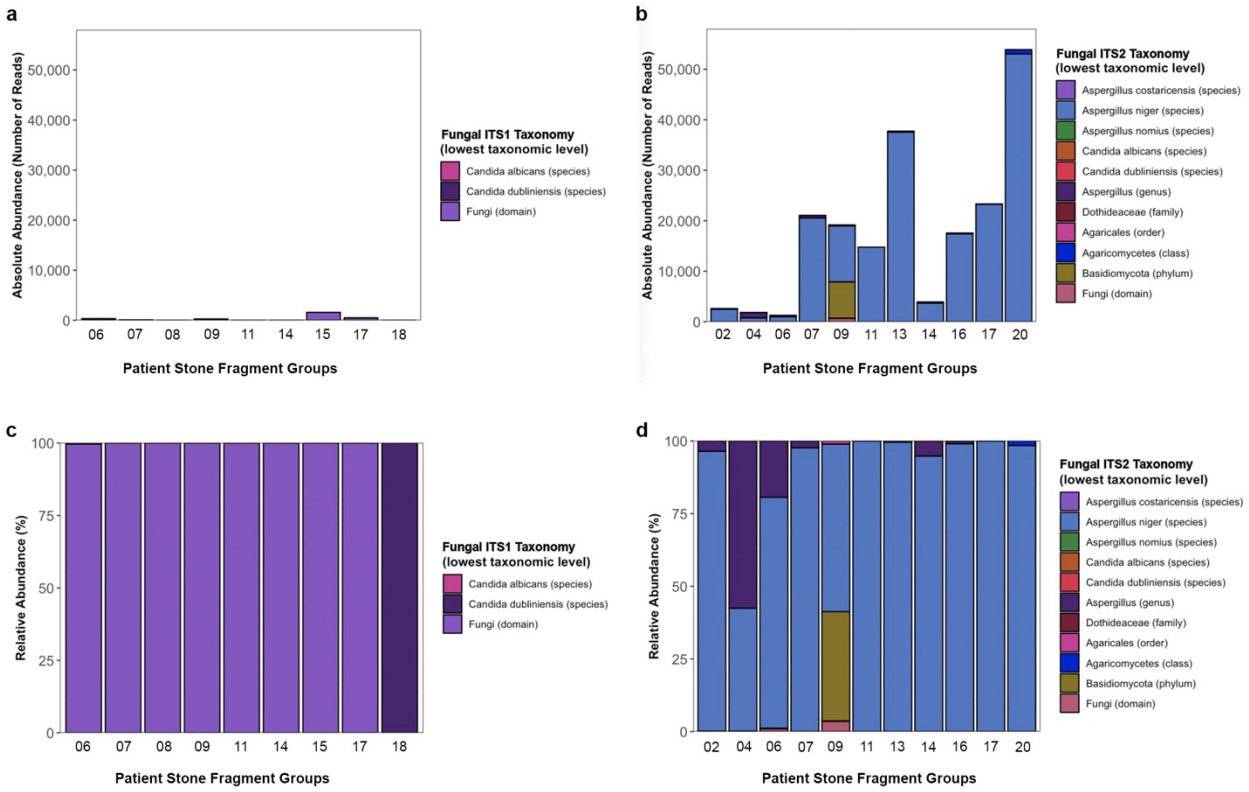

Figure S3. Comparison of ITS region fungal amplicon gene sequencing (ITS1 versus ITS2 region). Reads were identified in 9 stone fragment groups in the ITS1 amplicon sequencing versus 11 stone fragment groups in the ITS2 amplicon sequencing. Each individual stone fragment group is represented by an identification number (x-axis). (**a**, **b**) Absolute abundance of reads for each individual stone fragment group utilizing the ITS1 (**a**) and ITS2 (**b**) hypervariable regions. (**c**, **d**) Relative abundance of reads for each individual stone fragment group utilizing the ITS1 (**c**) and ITS2 (**d**) hypervariable regions.

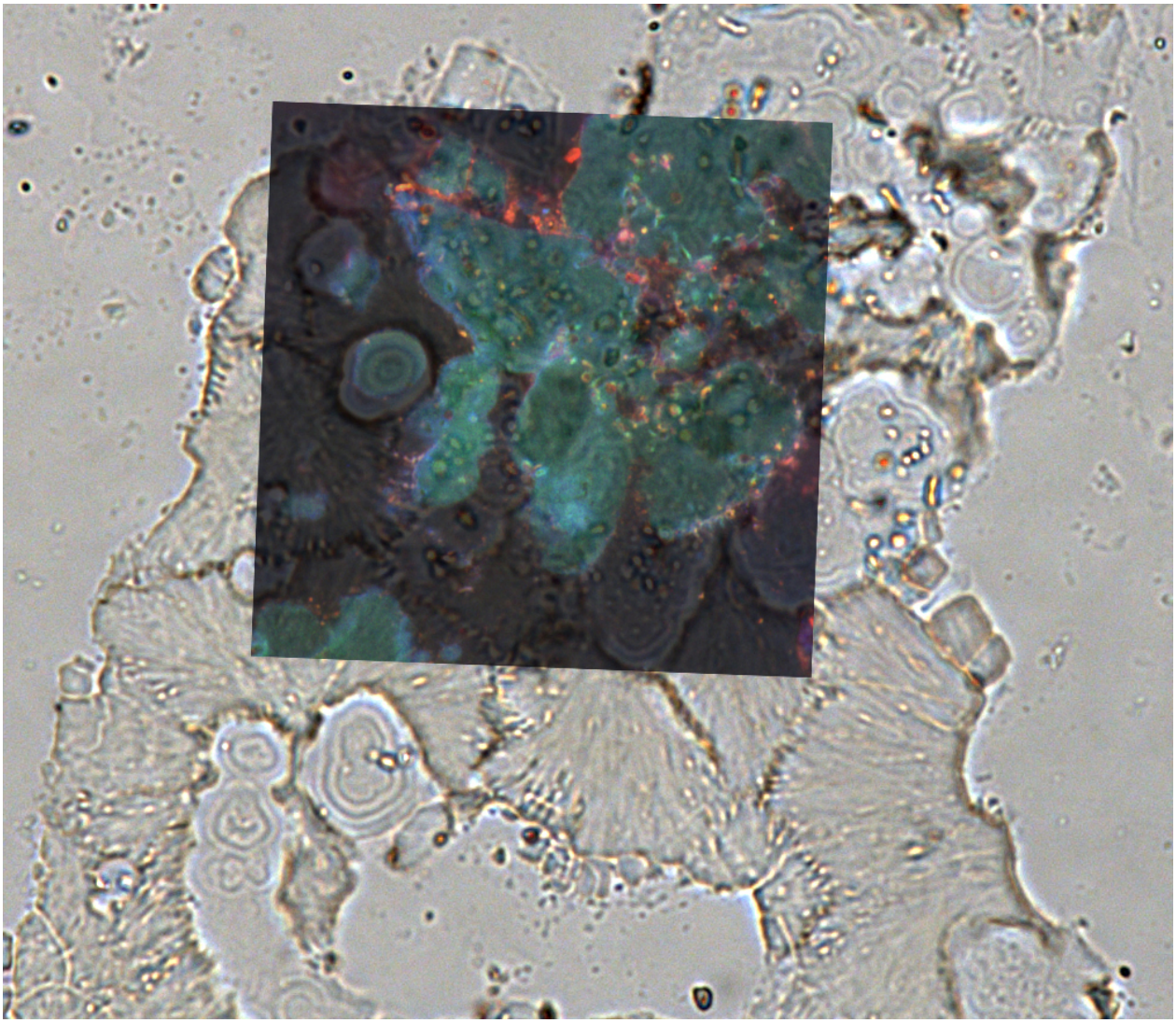

Figure S4. Overlay of SRAF image transparency on a larger field of view brightfield (BF) image. Note coccoidal and rod-shaped bacteria entombed in hydroxyapatite spherules and acicular struvite crystals within a struvite stone. See also Figure 5.

III. Supplementary Tables

Table S1. Demographic and clinical characteristics of patients

Patient Characteristics	**CaOx Stone Former *(n=18)***	**Struvite Stone Former *(n=1)***	**Brushite Stone Former *(n=1)***
Age ***(years)***	Average: 60.6 Min: 27 Max: 84	63	41
Sex ***(number of patients)***	Female: 11 Male: 7	Female: 0 Male: 1	Female: 0 Male: 1
Race ***(number of patients)***	Caucasian: 18	Caucasian: 1	Caucasian: 1
BMI ***(kg/m^2)***	Average: 35.4 Min: 21.0 Max: 53.9	28.8	24.3
Prior History of Kidney Stones ***(number of patients)***	Yes: 15 No: 3	Yes: 1 No: 0	Yes: 1 No: 0
Co-Morbidities ***(number of patients)***	HTN: 8 DMII: 2 MD: 4 Gout: 0 dRTA: 0	HTN: 1 DMII: 1 MD: 0 Gout: 0 dRTA: 0	HTN: 0 DMII: 0 MD: 0 Gout: 0 dRTA: 0
Medications ***(number of patients)***	Thiazides: 3 Citrate: 0 Allopurinol: 0	Thiazides: 0 Citrate: 0 Allopurinol: 0	Thiazides: 1 Citrate: 0 Allopurinol: 0

Abbreviations: CaOx = Calcium Oxalate, BMI = Body Mass Index, MD = Malabsorption disease, HTN = Hypertension, DMII = Diabetes Mellitus II, dRTA = distal renal tubular acidosis

Table S2. 24-hour Urine Supersaturation Profile

Patient ID	Osmolality (mOsm/kg)	pH	SS, CaOx (DG)	SS, Brushite (DG)	SS, Hydroxyapatite (DG)	SS, Uric Acid (DG)	SS, Sodium Urate (DG)
MP01	651	5.4	1.52	1.37	6.37	-1.98	2.26
MP02	769	5.6	2.47	0.84	4.78	3.31	2.56
MP03	821	5.2	2.79	0.95	3.79	4.15	2.8
MP04	607	5.5	1.97	1.27	5.25	1.38	2.13
MP05	321	7.1	1.12	0.77	6.05	-2.78	1.61
MP06	248	6.6	1.9	1.31	7.24	-4.75	1.21
MP07	522	5.8	NV	NV	NV	NV	NV
MP08	500	7.4	2.47	0.6	4.8	-0.1	0.48
MP09	460	6.8	2.31	-0.17	2.87	3.65	0.91
MP10	400	5.8	NV	NV	NV	NV	NV
MP11	NV	NV	1.66	-0.54	2.69	2.01	1.74
MP12	784	5.8	1.12	-1.34	2.89	-0.97	1.08
MP13	488	6	1.9	0.96	4.3	2.23	1.32
MP14	273	5.7	2.23	0.63	3.69	3.67	1.44
MP15	236	6.5	NV	NV	NV	NV	NV
MP16	454	6.9	1.33	0.91	6.06	-4.21	0.21
MP17	725	5.5	2.26	-0.48	2.54	3.1	1.46
MP18	614	5.1	1.32	-1.68	1.11	2.84	0.44
MP19	441	5.6	0.84	-3.08	-0.05	0.65	0.05
MP20	697	6.5	2.45	1.67	4.75	3.73	1.49
Average	**527**	**6.0**	**1.86**	**0.23**	**4.07**	**0.94**	**1.36**

Abbreviations: MP = Mayo Patient, SS = Supersaturation, DG = Delta G

Table S2, continued. 24-hour Urine Supersaturation Profile

Patient ID	Na^+ (mmol/ 24 hrs)	K^+ (mmol/ 24 hrs)	Ca^{2+} (mg/ 24 hrs)	Mg^{2+} (mg/ 24 hrs)	Cl^- (mmol/ 24 hrs)	PO_4^{3-} (mg/ 24 hrs)	SO_4^{2-} (mmol/ 24 hrs)	Citrate, (mg/ 24 hrs)	Oxalate (mmol/ 24 hrs)	Uric Acid (mg/ 24 hrs)	Cr (mg/ 24 hrs)
MP01	211	68	210	134	175	1070	25	643	0.26	651	1132
MP02	50	18	172	77	48	301	6	761	0.11	543	1074
MP03	101	27	204	44	86	662	9	931	0.14	339	1188
MP04	52	41	121	50	47	558	15	412	0.12	396	744
MP05	158	67	171	69	139	774	28	281	0.22	684	1476
MP06	239	64	293	148	219	933	16	<58	0.44	788	1954
MP07	NV	NV	NV	NV	NV	NV	NV	NV	NV	NV	NV
MP08	110	57	410	239	110	569	9	1035	0.31	440	1101
MP09	101	28	387	85	104	838	15	857	0.21	712	1724
MP10	NV	NV	NV	NV	NV	NV	NV	NV	NV	NV	NV
MP11	397	116	267	235	410	1674	22	775	0.54	891	2673
MP12	172	80	109	71	164	663	19	1002	0.45	507	1268
MP13	87	41	247	117	51	957	16	449	0.14	462	924
MP14	123	68	551	96	126	800	15	1175	0.14	575	1413
MP15	NV	NV	NV	NV	NV	NV	NV	NV	NV	NV	NV
MP16	159	75	279	108	138	936	17	684	0.26	442	1508
MP17	235	51	446	144	218	994	24	1566	0.32	694	1838
MP18	118	70	122	89	82	1140	24	333	0.32	627	1292
MP19	259	46	55	148	216	1311	10	113	0.92	567	1382
MP20	46	29	261	107	50	870	13	281	0.11	452	1626
Average	**154**	**56**	**253**	**115**	**140**	**885**	**17**	706	0.29	575	1430

Abbreviations: MP = Mayo Patient, Cr = Creatinine

Table S3. Full IR Spectroscopy Results

Patient ID	Apatite (%)	COM (%)	COD (%)	Struvite (%)	Brushite (%)	Final Clinical Identification of Mineralogy
MP01	90	10	-	-	-	CaOx
MP02	-	100	-	-	-	CaOx
MP03	20	80	-	-	-	CaOx
MP04	-	100	-	-	-	CaOx
MP05	10	60	30	-	-	CaOx
MP06	-	-	-	100	-	Struvite
MP07	-	100	-	-	-	CaOx
MP08	20	20	60	-	-	CaOx
MP09	10	20	70	-	-	CaOx
MP10	5	-	95	-	-	CaOx
MP11	-	100	-	-	-	CaOx
MP12	-	90	10	-	-	CaOx
MP13	-	100	-	-	-	CaOx
MP14	-	100	-	-	-	CaOx
MP15	30	10	60	-	-	CaOx
MP16	-	100	-	-	-	CaOx
MP17	-	90	10	-	-	CaOx
MP18	20	80	-	-	-	CaOx
MP19	-	100	-	-	-	CaOx
MP20	10	-	-	-	90	Brushite

Abbreviations: COM = Calcium Oxalate Monohydrate, COD = Calcium Oxalate Dihydrate, CaOx = Calcium Oxalate

Table S4. Read Summary for16S rRNA (V1-V3 and V3-V5 hypervariable region) and ITS (ITS1 and ITS2 regions) Amplicon Gene Sequencing

	V1-V3	V3-V5	ITS1	ITS2
Patient Stone Fragment Groups				
Number of Patient Groups	6	9	9	11
Total Number of Reads	276,979	309,486	2,726	197,004
Total Number of Unique ASVs	135	214	11	153
Average Number of Reads per Sample	46,163.17	34,387.33	302.89	17,909.45
CaOx Stone Fragment Groups				
Number of Patient Groups	4	7	8	9
Total Number of Reads	20,985	215,234	2,411	141,872
Total Number of Unique ASVs	54	149	9	124
Average Number of Reads per Sample	5,246.25	30,747.71	301.38	15,783.55
Brushite Stone Fragment Group				
Number of Patient Groups	1	1	*NA	1
Total Number of Reads	18,059	63,327	NA	53,873
Total Number of Unique ASVs	11	36	NA	26
Average Number of Reads per Sample	NA	NA	NA	NA
Struvite Stone Fragment Group				
Number of Patient Groups	1	1	1	1
Total Number of Reads	237,935	30,925	315	1,259
Total Number of Unique ASVs	70	40	2	8
Average Number of Reads per Sample	NA	NA	NA	NA

*ITS1 region amplicon gene sequencing in the brushite stone fragment cohort detected no fungal reads.

V. Supplementary References

1. Sivaguru M, Saw JJ, Williams JC, Lieske JC, Krambeck AE, Romero MF, et al.: Geobiology reveals how human kidney stones dissolve in vivo. *Scientific Reports,* 8**:** 1-9, 2018 10.1038/s41598-018-31890-9
2. Smith LH: *Diseases of the Kidney*, Fourth Edition Ed., Boston, MA, Little, Brown and Company, 1987
3. GBD CKDC: Global, regioal, and national burder of chroic kidney disease, 1990-2017: a systemtic analysis for the Global Burden of Disease Study 2017. *The Lancet,* 395**:** 709-733, 2020 https://doi.org/10.1016/S0140-6736(20)30045-3
4. Callahan BJ, McMurdie PJ, Rosen MJ, Han AW, Johnson AJ, Holmes SP: DADA2: High-resolution sample inference from Illumina amplicon data. *Nat Methods,* 13**:** 581-583, 2016 10.1038/nmeth.3869
5. Graessler J, Mehnert CS, Schulte KM, Bergmann S, Strauss S, Bornstein TD, et al.: Urinary Lipidomics: evidence for multiple sources and sexual dimorphism in healthy individuals. *Pharmacogenomics Journal,* 18**:** 331-339, 2018 10.1038/tpj.2017.24
6. Nilsson RH, Larsson KH, Taylor AFS, Bengtsson-Palme J, Jeppesen TS, Schigel D, et al.: The UNITE database for molecular identification of fungi: handling dark taxa and parallel taxonomic classifications. *Nucleic Acids Research,* 47**:** D259-D264, 2019 10.1093/nar/gky1022
7. McMurdie PJ, Holmes S: phyloseq: An R Package for Reproducible Interactive Analysis and Graphics of Microbiome Census Data. *PLoS ONE,* 8**:** e61217, 2013 10.1371/journal.pone.0061217
8. Team RC: R: A language and environment for statistical computing. R Foundation for Statistical Computing. 2013
9. Sivaguru M, Urban MA, Fried G, Wesseln CJ, Mander L, Punyasena SW: Comparative performance of airyscan and structured illumination superresolution microscopy in the study of the surface texture and 3D shape of pollen. *Microsc Res Techniq,* 81**:** 101-114, 2018 10.1002/jemt.22732
10. Kolossov VL, Sivaguru M, Huff J, Luby K, Kanakaraju K, Gaskins HR: Airyscan super-resolution microscopy of mitochondrial morphology and dynamics in living tumor cells. *Microsc Res Techniq,* 81**:** 115-128, 2018 10.1002/jemt.22968
11. Takasaki E: Carbonate in struvite stone detected in Raman spectra compared with infrared spectra and X-ray diffraction. *Int J Urol,* 3**:** 27-30, 1996 10.1111/j.1442-2042.1996.tb00625.x
12. Balan V, Mihai CT, Cojocaru FD, Uritu CM, Dodi G, Botezat D, et al.: Vibrational Spectroscopy Fingerprinting in Medicine: from Molecular to Clinical Practice. *Materials (Basel),* 12, 2019 10.3390/ma12182884
13. Cromey DW: Avoiding Twisted Pixels: Ethical Guidelines for the Appropriate Use and Manipulation of Scientific Digital Images. *Science and Engineering Ethics,* 16**:** 639-667, 2010 10.1007/s11948-010-9201-y